# Nanoscale Networks of Metal Oxides by Polymer Imprinting and Templating for Future Adaptable Electronics

Berg, Alexandra; Jonkman, Harry; Loos, Katja; Portale, Giuseppe; Noheda, Beatriz

Link to publication in University of Groningen/UMCG research database

# Novel MXene sensors based on fast healing vitrimers

Chongnan Ye [a],[1], Feng Yan [b],[1], Xiaohong Lan [a], Petra Rudolf [b], Vincent S.D. Voet [c], Rudy Folkersma [c], Katja Loos [a],*

[a] Macromolecular Chemistry and New Polymeric Materials, Zernike Institute for Advanced Materials, University of Groningen, Nijenborgh 4, Groningen 9747 AG, the Netherlands
[b] Surfaces and Thin Films, Zernike Institute for Advanced Materials, University of Groningen, Nijenborgh 4, Groningen 9747 AG, the Netherlands
[c] Professorship Sustainable Polymers, NHL Stenden University of Applied Sciences, Van Schaikweg 94, Emmen 7811 KL, the Netherlands

## ARTICLE INFO

## ABSTRACT

Soft matter containing $Ti_3C_2T_x$ MXenes exhibits promising potential in electromechanical sensor development. Current systems suffer from a decrease in sensibility up to complete breakdown due to small structural defects that will be generated during their longtime practical service. Various non-covalent hydrogel systems, based on hydrogen bonding and ionic coupling, have been employed to improve their durability related to their repairability. However, $Ti_3C_2T_x$ MXenes are not stable in those networks, since they will be irreversibly oxidized in high humidity environment during practical application. Here, we report the use of a novel dynamic covalent bond based network – a MXene acrylate vitrimer network (MAVIN) with a low glass transition temperature, which can not only be repaired fast with high efficiency but also protects the MXenes in sensor applications from oxidation under working conditions. In addition, owing to the strong microwave absorptivity of $Ti_3C_2T_x$ and of the flexible dynamic covalent bond network, a damaged MAVIN sensor can be repaired by microwave radiation with a high healing efficiency of 92.4% within 1 minute, which is as good as the best healing efficiency reported in literature so far but 30 times faster. With stability at a voltage of 3 V and fast healing demonstrated, MAVIN promises potential usage in reliable and sustainable strain sensors.

## 1. Introduction

MXenes, that belong to a novel class of 2D materials, have been widely studied in the last decade [1,2]. $Ti_3C_2T_x$ received tremendous attention concerning its potential for application in numerous fields [3–8], such as lithium battery fabrication [9,10], supercapacitor development [11,12], smart window design [13], and hydrogen production [14,15]. When external stress or pressure is applied, the interlayer distance of $Ti_3C_2T_x$ flakes substantially changes, which leads to large resistance variations, resulting in a high strain sensitivity [16]. This characteristic of soft $Ti_3C_2T_x$ hybrid materials opens promising prospects for wearable strain sensor fabrication.

Flexible and largely deformative wearable strain sensors attract a lot of attention to mimic biological systems, *e.g.* soft robotic construction [17,18]. However, due to their inherent working mechanism, large deformations usually generate small structural defects, which severely impact their longevity and performance [19], leading to a decrease of

sensibility of the sensor till breakdown. Repair mechanisms like healing are crucial in sensor development to guarantee a longtime reliable service. The majority of currently reported healing MXene sensors are currently based on supramolecular non-covalent chemistry such as hydrogen bonding or ionic interactions [20–23].

Despite their potential, $Ti_3C_2T_x$ devices based on non-covalent interactions remain vulnerable in real-world applications, because MXene is prone to chemical degradation by oxidation. The current healing MXene hydrogel sensors [24], based on hydrogen bonding or ionic interactions, face even more severe challenges since they face irreversible oxidation [25]. Once MXene is oxidized, the sensor loses its functionality but this issue for practical applications has not been addressed until now [26,27]. To prevent the oxidation of MXene and improve (mechanical) stability of the sensor, a solvent-free healing sensor is required.

Vitrimers, a new class of polymeric materials developed in recent years, consisting of polymer networks crosslinked by dynamic covalent bonds [28,29], provide a solution for this problem. Similar to classical

thermosets, vitrimers are robust materials [29–32] but feature also a unique healing ability, owing to bond-exchange reactions [31–38]. Despite those advantages, the majority of vitrimers are rigid and need high temperatures to trigger bond exchange reactions (> 100 °C for a polyester-based network for example) [39] as well as long healing times (often over 24 h) [30,39]. However, for breaking and reconstructing the ester bond, the transesterification mechanism itself actually takes place already at 60 °C [40].

Here we report a new type of material - a MXene acrylate vitrimer network (MAVIN) - that relies on two different and at times synergistic characteristics to achieve fast healing. Firstly, the flexible siloxane backbone (PDMS) engenders a low glass transition temperature, above which the increasing number of collision events between free hydroxyl groups and ester bonds speeds up bond exchange reactions [41]. Secondly, a large concentration of hydroxyl groups, particularly in the proximity of ester bonds ($\beta$-hydroxyl ester), built into this vitrimer network via incorporated acrylate groups, also significantly accelerates the transesterification rate [42].

Esterification usually requires heating to be activated but MXene is extremely sensitive to oxygen at high temperatures and in the presence of a solvent [43]. To prevent oxidation of MXene during the curing process, a thiol-Michael addition reaction was chosen to synthesize MAVIN since it can take place under moderate conditions. To introduce the necessary double bonds and the $\beta$-hydroxyl esters, short chain poly (dimethylsiloxane) diacrylate (AA-PDMS) was synthesized to act as a precursor to form MAVIN. In contrast to the traditional non-polar acrylate PDMS, the presence of $\beta$-hydroxyl groups in AA-PDMS enables the dissolution in ethanol and thereby a homogeneous mixture with the MXene suspension.

To produce MAVIN with well-dispersed MXene, short chain AA-PDMS, short chain AA-PEG and ethylene glycol (EG) were first dissolved in a MXene ethanol solution. Subsequently, an organogel was achieved by crosslinking AA-PDMS and AA-PEG with a 4-arm thiol crosslinker (tetra (3-mercaptopropionate) (PETMP)) under mild conditions (Fig. 1a). Here, triazabicyclodecene (TBD) not only acts as catalyst for the thiol-Michael addition reaction in this curing process but also facilitates transesterification reactions at elevated temperature (> 60 °C), which enables the cured network to rearrange its topology by bond exchange reactions during later healing steps. The PEG backbone interacts with free EG molecules, and therefore enables MAVIN to retain EG within the network during its preparation. Hence, it is a vital part of the formulation, since EG will introduce the dangling hydroxyl groups and generate topological defects in the network during solvent evaporating at high temperature (100 °C) (Fig. 1b). As a result, a piece of solvent-free MAVIN with flexible dangling chains comprising OH endgroups was obtained.

Compared to previously reported rigid vitrimer systems, the topological defects and flexible (siloxane) moieties endow our network with higher flexibility, which is crucial not only for fast healing, but also for potential application in a wearable strain sensor. Meanwhile, the welldispersed $Ti_3C_2T_x$ flakes in MAVIN can efficiently heat to activate the dynamic bond exchange under microwave radiation since $Ti_3C_2T_x$ is a strong microwave absorber [44].

## 2. Materials and methods

### 2.1. Materials

Pentaerythritol Tetra(3-mercaptopropionate) (PETMP, 90 %) and Polyethylene Glycol Diacrylate (n=approx. 14, AA-PEG) were purchased from Tokyo Chemical Industry. Poly(dimethylsiloxane) (PDMS, Mn ~ 800, diglycidyl ether terminated), triazabicyclodecene (TBD, 98



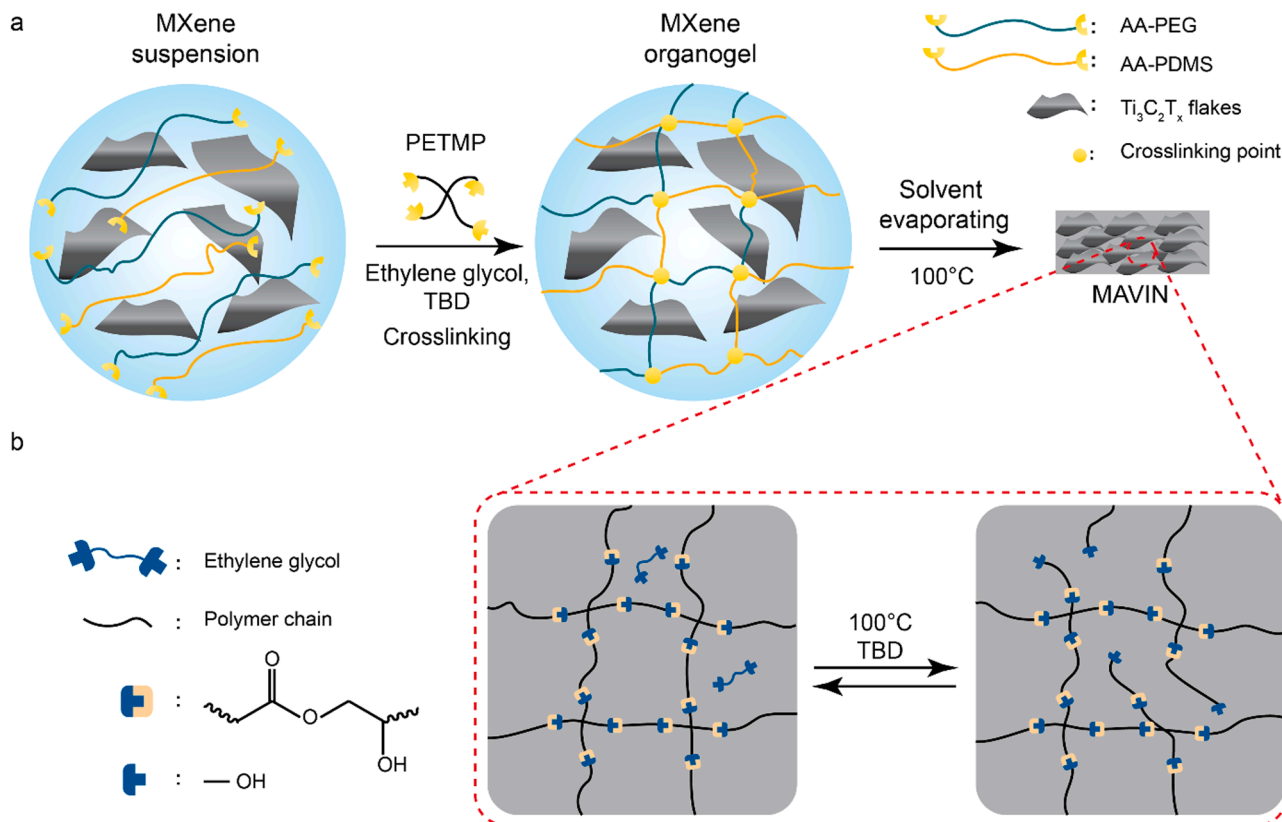**Fig. 1.** Design of $Ti_3C_2T_x$ vitrimer sensors. a Schematic illustration of the MXene acrylate vitrimer network (MAVIN) preparation, using thiol-Michael addition. b Schematics of the mechanism of transesterification inside the dynamic covalent bonding network that occurs during solvent evaporation, introducing dangling chains with hydroxyl end-groups.

%), acrylic acid (99 %), 4-methoxyphenol (MEHQ, 99 %), triphenyl-phosphine (TPP, 99 %), poly(vinyl alcohol) (PVA, $M_w$ 146,000~186,000, 99 % hydrolyzed), NaHCO$_3$ (99 %), sodium tetra-borate (99 %), ethylene glycol (99 %), lithium fluoride(powder, -300 mesh) and silver conductive paste were purchased from Sigma-Aldrich. Aceton (HPLC grade), ethanol (HPLC grade), dichloromethane (DCM, HPLC grade) and hydrochloric acid (37 %) were supplied by Boom B.V. MAX phase powder (Ti$_3$AlC$_2$, particle size $\leq$ 40 µm) was acquired from Y-Carbon Ltd., Ukraine. Milli-Q water (resistivity 18 MΩ·cm, 25 °C) was freshly produced before use. All the chemicals were used as received.

### 2.2. AA-PDMS and Ti$_3$C$_2$T$_x$ synthesis

PDMS-diglycidyl ether terminated (16 g, 20 mmol), acrylic acid (5.76 g, 80 mmol), triphenylphosphine (1 % w/w, 0.22 g) and MEHQ (0.2 % w/w, 0.045 g) were added in a 100 mL round bottom flask. The mixture was stirred at 105 °C for 16 h. After completion, the reaction

was diluted with 50 mL of DCM and washed with a 5 % sodium bicar-bonate aqueous solution (200 mL, three times). Then the excess solvent was evaporated under an air flow to yield the final product (Yield: 17.93 g, 94.97%). $^1$H-NMR (600 MHz, CDCl$_3$, δ): 6.45, 6.18, 5.85 (3H, CH$_2$=CH-), 4.49-3.46 (5H, CH and CH$_2$), 1.60 (2H, CH$_2$), 0.52 (2H, CH$_2$), 0.05(27H, CH$_3$) (Fig. 2b).

Ti$_3$C$_2$T$_x$ was synthesized by etching of the Al atomic layers from the MAX (Ti$_3$AlC$_2$) phase. For this, 8.0 g of LiF was added slowly to 100 mL HCl (9.0 M) while magnetically stirring for 30 min, then 5.0 g of Ti$_3$AlC$_2$ powder was slowly added to the solution. Next, the mixture was stirred at 350 rpm for 24 h at 40 °C. After reaction, the mixture was repeatedly washed with Milli-Q water, and centrifuged at 4500 rpm for 10 min until a deep dark supernatant and a swollen sediment were observed. Then the sediment was redispersed in 200 mL of Milli-Q water and sonicated in an ice bath with Ar flow for 2 h. Following, the mixture solution was centrifuged at 3500 rpm for 1 h and the turbid upper black liquid was collected. By washing several times with Milli-Q water, the pH of the
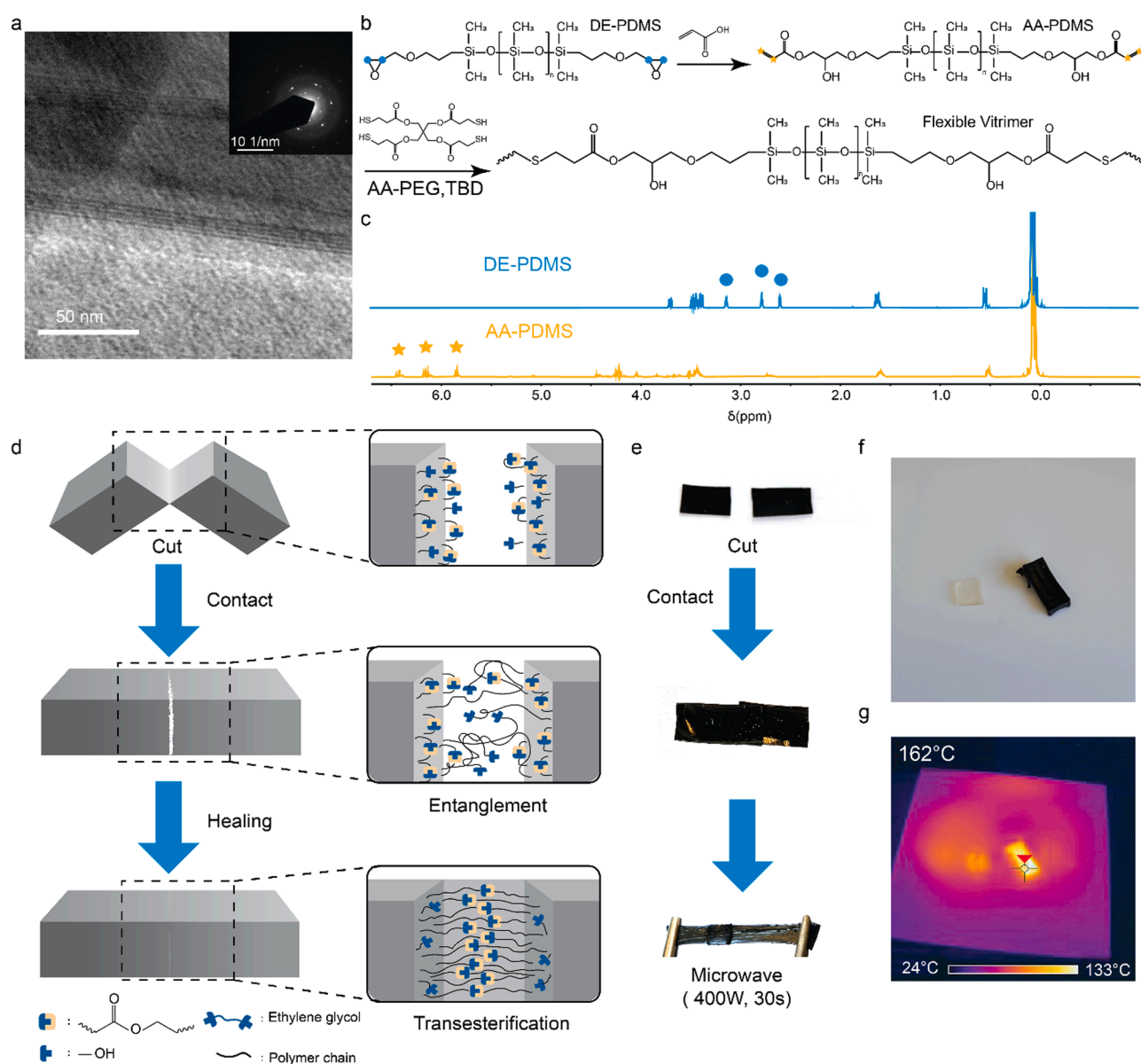


**Fig. 2.** Characterization and mechanical healing performance of a Ti$_3$C$_2$T$_x$ vitrimer sensor. a high-resolution TEM image of the exfoliated Ti$_3$C$_2$T$_x$ nanosheet (Inset: Corresponding SAED of MXene). b Synthetic approach for the preparation of AA-PDMS and crosslinking of the AA-PDMS *via* thiol-Michael reaction. c $^1$H NMR spectra of the DE-PDMS and corresponding AA-PDMS. d Illustration of the healing process of MAVIN. e Photographic images during the course of the healing experiment of MAVIN, under microwave for 30 s. f and g Ordinary photograph and infrared thermal imaging of MAVIN and blank contrast with 60 s of microwave irradiation.

supernatant was brought to 5.5, where after the $Ti_3C_2T_x$ flakes were collected by centrifugation at 12,000 rpm and vacuum dried at room temperature overnight. The dry black powder was stored in a vacuum desiccator until further use.

### 2.3. Fabrication of stretchable and healable MAVIN and MHS

MAVIN was obtained by a straightforward process: first AA-PDMS (0.47 g, 0.5 mmol), AA-PEG (0.346 g, 0.5 mmol), ethylene glycol (7 μL) and TBD (10 mg) were dissolved in 2 mL $Ti_3C_2T_x$ ethanol solution (4 mg/mL) to obtain AA $_{solution}$. Then PETMP (0.24 g, 0.5 mmol) was first dissolved in 400 μL acetone and then diluted with the same 1.6 mL $Ti_3C_2T_x$ ethanol solution to get SH $_{solution}$. Finally, by mixing AA $_{solution}$ and SH $_{solution}$ in a PTFE mold, a piece of MAVIN was obtained after solvent evaporation.

The MHS system was produced according to the protocol developed by Liao et al. [21]: 0.8 g PVA powder was added to 9 g Milli-Q water under vigorous stirring at 90 °C for 2 h to form a PVA solution. Subsequently, 1.0 g $Ti_3C_2T_x$ aqueous solution (4 mg/mL) and 2.0 g PVA solution, were mixed together. After that, 500 μL borax solution (4 wt%) was added dropwise under stirring until a hydrogel was obtained.

### 2.4. Healing, tensile testing and electromechanical (sensor) measurements

We characterized the mechanical properties of hybrid elastomers using a Low Force Universal Testing Systems Instron 5565 (USA) with a 100 N load cell. Samples were cut from the film that had been peeled off from the PTFE mold. The samples have a dimension of 21 mm in length, 5 mm in width, and 0.23 mm in thickness. Mechanical tensile stress and mechanical healing tests were performed at room temperature with a stain rate of 10 mm/ min. Damaged samples were given 30 s or 60 s to heal under 400 W microwave irradiation. Cyclic extension tests were performed on the same tensile machine cycling ten times with a maximum of 20 % strain at a strain rate of 10 mm/ min. A minimum of three specimens per sample were analyzed.

Electromechanical measurements were performed on MAVIN sensor samples using a Rigol DS1054 setup in the two-probe mode. To fabricate MAVIN sensors, a stripe of MAVIN was integrated into the circuit by using copper foil and silver paste. For gauge factor tests, the specimens were strained at a rate of 10 mm/min until reaching a breaking strain of ~103 %. During electromechanical tests, contact was made by using silver paste and copper tape to place the wire at the end of the sample.

### 2.5. $Ti_3C_2T_x$ sample preparation for XPS measurements

$Ti_3C_2T_x$ MAVIN (3V): As the concentration of $Ti_3C_2T_x$ is too low in MAVIN to be detected by XPS, after applying 3 V for 18 h, the sample was first depolymerized with 1 mL ethylene glycol and 4 mL ethanol at 55 °C for 30 min. The MXene was then collected by centrifugation (14,000 rpm, 10 min). Following three times washing with ethanol, the $Ti_3C_2T_x$ flakes were finally collected and dispersed in the ethanol to achieve a suitable concentration for XPS sample preparation.

$Ti_3C_2T_x$ MHS (3 V): The liquid MHS sample was obtained by abandoning the borax solution. Following the oxidation test, the liquid MHS sample was directly used for XPS investigation.

In each case the dispersion was drop-casted on a homemade [45] 150 nm thick gold film was supported on mica and dried in air before being introduced in UHV for XPS measurements.

### 2.6. Material characterization

Nuclear Magnetic Resonance (NMR) spectra were recorded on a Bruker Avance II 400 or Bruker Ascend 600 FT-NMR spectrometer at 25 °C in the deuterated solvent as indicated.

Infrared (IR) images were captured with a FLIR i7 infrared camera.

Differential Scanning Calorimetry (DSC) was carried out on a TA DSC

Q1000 instrument in a dry $N_2$ atmosphere. Samples were analyzed in a range from -90 °C to 180 °C by performing heating-cooling-heating scans with heating and cooling rates of 10 °C/min.

The morphology, size distribution, and SAED of $Ti_3C_2T_x$ were analyzed by transmission electron microscopy (TEM, JEOL 2010) operating at 200 kV. XPS was performed with an SSX-100 (Surface Science Instruments) spectrometer equipped with a monochromatic Al Kα X-ray source (hν = 1486.6 eV). The pressure in the measurement chamber was maintained at $1 \times 10^{-9}$ mbar during data acquisition; the photoelectron take-off angle was 37° with respect to the surface normal. Spectral analysis, including Shirley background subtraction and fitting, was performed utilizing least squares curve-fitting program WinSpec (LISE, University of Namur, Belgium) and peak profiles as a convolution of Gaussian and Lorentzian functions. Binding energies were referenced to the $Au4f_{7/2}$ peak [46] at 84.0 eV and are accurate to ±0.1 eV when deduced from the fitting procedure. All measurements were carried out on freshly prepared samples; three different spots were measured on each sample to check for homogeneity.

XRD spectra were acquired using a D8 Advance Bruker diffractometer with Cu Kα radiation (λ = 1.5418 Å) employing a 0.25° divergent slit and a 0.125° anti-scattering slit; the patterns were recorded in the 2θ range from 2° to 80°, in steps of 0.02° and a counting time of 2 s per step.

## 3. Results and discussion

### 3.1. Preparation and characterization of $Ti_3C_2T_x$ and $Ti_3C_2T_x$ nanocomposites

Selective etching of $Ti_3AlC_2$ (MAX phase), followed by exchanging the dispersant from water to ethanol [47], yielded a stable ethanol dispersion of $Ti_3C_2T_x$. As can be seen from the X-ray photoelectron spectroscopy (XPS) data presented in the Supplementary information Fig. S1, all the elements expected after the etching process are present in the right proportions, and the detailed photoemission spectra of the O1*s,* F1*s,* Ti2*p,* and C1*s,* core level regions confirm that there are abundant functional groups at the surface of the MXene flakes, including hydroxyl groups, carbonyl groups and fluorine [48].

The structure of MXene was examined by transmission electron microscopy (TEM) and X-ray diffraction (XRD). The micrograph in Fig. 2(a) unambiguously reveals the presence of well-etched $Ti_3C_2T_x$ nanosheets. The selected area electron diffraction (SAED, inset in Fig. 2(a) exhibits a typical hexagonal symmetry diffraction pattern, indicating the high crystallinity of a typical MXene nanosheet (Fig. 2a) [49]. Its lateral diameter is several hundred of nanometers, which matches the flake size distributions of MXene reported in the literature [13]. From the XRD peak located at 6.12° (001) an interlamellar distance of 1.51 nm is deduced for the MXene (Fig. S2).

To fabricate a stretchable vitrimer network, AA-PDMS was synthesized by the reaction of acrylic acid with diepoxidized PDMS (DE-PDMS) (Fig. 2b) [34]. A successful substitution is confirmed using ^{1}H-NMR, where, as indicated in the spectrum in Fig. 2c, the signal of acrylate double bonds (6.39, 6.11 and 5.82 p.p.m.) was detected while the epoxy-related signals (3.12, 2.77 and 2.58 p.p.m.) vanished. In addition,^{13}C-NMR, HSQC and FTIR spectrometry were employed to confirm full conversion (Figs. S3 and S4). Due to its polarity, AA-PDMS is solvable in the $Ti_3C_2T_x$ ethanol suspension, which is crucial to obtain a well dispersed MXene vitrimer network.

The network was formed by reacting the defined quantities of the acrylate monomers (AA-PDMS and AA-PEG) with pentaerythritol tetra (3-mercaptopropionate) (PETMP) and ethylene glycol (EG) in the $Ti_3C_2T_x$ ethanol suspension (Fig. 1a and Methods). Following a solvent evaporation process, the quantified EG (0.125 to the thiol group molar ratio) was utilized to cleave ester bonds to create dangling chains in the MAVIN (Fig. 1b and Methods). During this process, TBD acts as a catalyst not only to activate the transesterification but also to increase the rate of crosslinking.

### 3.2. Mechanical properties of MAVIN, before and after healing through dynamical covalent bond exchange reactions

Owing to flexible PDMS and the PEG-based polymeric backbone, our vitrimer network exhibits a low glass transition temperature ($T_g = -47.9°C$) (Fig. S5), which warrants high stretchability at room temperature. The MAVIN exhibited a tensile stress of 130 KPa at a maximum strain (Fig. 3a). Additionally, unlike other MXene hydrogen bonding networks [50], there is no obvious hysteresis observed during a 200 cycles tensile loading-unloading test of MAVIN, which indicates excellent stability of the network bearing strain under ambient environment (Fig. 3b). Moreover, due to the bond exchange reactions within the network, the MAVIN possesses an excellent healing capability. To prove that, the elastomer was cut into two pieces that were subsequently placed on top of each other for reaction under microwave irradiation. The topological defects (intra-chain cycles or dangling chains) are expected to synergistically provide more entanglements at the damaged surface. The more polymer chains re-entangle, the more reconfiguration takes place (Fig. 2d). Benefiting from the well-dispersed $Ti_3C_2T_x$ flakes in the network, the as-prepared material shows a high microwave thermal conversion (Fig. 2f, g). Notably, it takes merely 30 s to reach 162 °C for the MAVIN, while the blank sample reaches 64°C at the same time. Therefore, the cut MAVIN was found to heal in less than 1 min as illustrated in the photographs in Fig. 2e. To further quantify the healing ability, tensile stress–strain experiments were carried out (Fig. 3a). The healing efficiency is defined as the ratio of the breaking stress of healed $Ti_3C_2T_x$ nanocomposites to the breaking stress of the pristine sample. For longer time irradiation, the tensile stress–strain curves show improved healing efficiency of the MAVIN, which is above 90 % after 1 minute of irradiation. Moreover, the healed MAVIN exhibited the same behavior during the 200 cycles tensile loading-unloading test, which confirms its excellent healing capability (Fig. 3b, c). The concentration of MXene plays a crucial role in the healing process as well as the mechanical properties. (Fig. S6) When we halved the amount of MXene, the MAVIN became more stretchy (strain= 197%) but it only can be healed 46.3% within 1 min by applying the same condition. In contrast to this, the MAVIN with doubled MXene content can be healed 93.5% within the 60 s and the network is stronger but rigid, which is unfavorable for strain sensors.

For practical applications, healing speed and healing efficiency are two crucial parameters that need to be considered for a reliable healing strain sensor. On the one hand, as dynamic covalent bond network, vitrimers typically demonstrate high healing efficiency, however, usually they are rigid and need a very long time, of the order of several hours, for effective healing [39]. On the other hand, elastomer networks based on non-covalent interaction (*i.e.* hydrogen bonds) can be healed in a very short time but show lower healing efficiency [21,23,50–52]. In contrast to systems reported until now, owing to the integration of dangling chain entanglements and fast bond exchange reactions, the designed MAVIN is flexible and exhibits a high healing efficiency (92.4 %) within 1 min, which is as good as the best healing efficiency reported so far but it can be reached 30 times faster than any system reported so far (Fig. 3d).
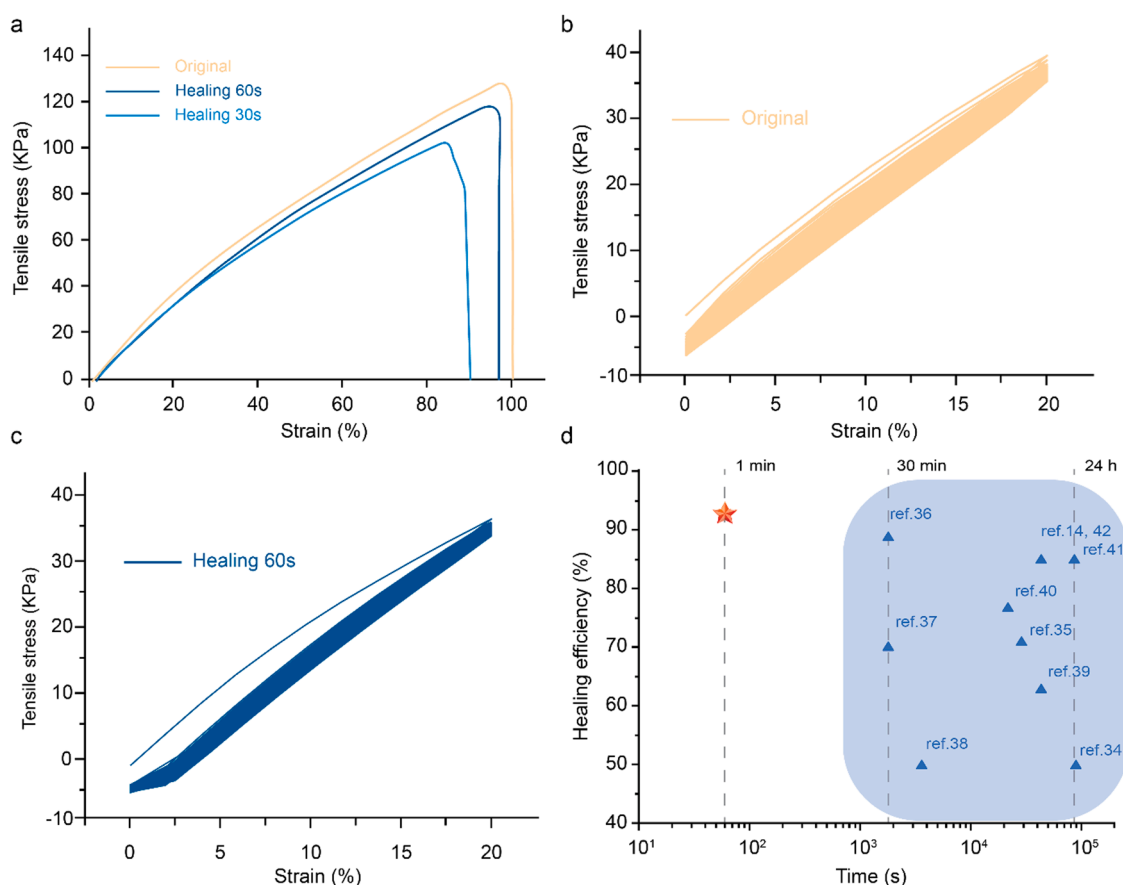


**Fig. 3.** Mechanical healing performance of a $Ti_3C_2T_x$ vitrimer sensor. a tensile stress–strain curves of the original and healed MAVIN – healing time 30 s and 60 s. Stress–strain curves of (b) pristine MAVIN, and (c) healed MAVIN during 200 cyclic loadings MAVIN with 20 % strain and 30 mm/min loading rate. d Ashby plot of healing efficiency versus healing time. MAVIN is highlighted by red star and the triangles refer to previously reported vitrimers and healing elastomers [21, 23,50–57].

### 3.3. Sensing Properties of the MXene-based healing electronic sensor

A stripe (5.8 mm × 12.7 mm × 1.0 mm) of the MAVIN was integrated into a closed circuit connected to a semiconductor characterization system, to work as a strain sensor (Methods). With strain applied, the interlayer distance of $Ti_3C_2T_x$ nanosheets in MAVIN changes, which in turn causes changes the resistance resulting an electrical signal variation. As an essential sensor property, the gauge factor (GF) was first investigated to evaluate the sensitivity corresponding to the variation of the strain. The GF is defined as: GF = d($\Delta R/R_0$)/d$\varepsilon$. Here, $\Delta R/R_0$ represents the relative resistance variation during deformation, $R_0$ is the electrical resistance when no strain is applied, and $\varepsilon$ is the strain. When the applied strain increases progressively, the relative resistance is found to increase almost linearly (GF ≈ 3.71) (Fig. 4a), causing a distinct drop in the electrical conductance. This phenomenon can be understood considering that when the $Ti_3C_2T_x$ flakes move apart they disconnect electronically. A cyclic strain test (from 0 % to 20 %) was carried out to evaluate the sensor`s durability and stability. Fig. 4b shows MAVIN responding to the loading−unloading cycles with an excellent stability and outstanding reproducibility for 200 cycles.

Additionally, MAVIN exhibits excellent stability under 20 % strain at frequencies ranging from 0.25 to 1 Hz. (Fig. S7). To demonstrate the potential application of MAVIN, a stripe (5.8 mm × 10.3 mm × 1 mm) of MAVIN was attached to a finger for real-time motion monitoring of finger bending. As shown in Fig. 4c, the relative resistance variation was uniform over many bending cycles.

The healed MAVIN was tested in the same fashion as the pristine one and found to not only show good (mechanical) recovery but also excellent stability and reproducibility of its functionality, as demonstrated in Fig. 4d–f in comparison to Fig. 4a–c. Such outstanding performance surpasses that of previously reported MXene-based sensors, leading to the conclusion that in terms of healing time and healing efficiency, two-key factors for healable stretchable sensors, MAVIN outperforms other healing MXene sensors [20,21,23,58,59].

### 3.4. Remarkable oxidation resistance of MAVIN under working conditions

A hydrogel has been the most common system for $Ti_3C_2T_x$ healing strain sensor fabrication in recent years [22]. Despite their promising properties, questions about MXenes chemical stability remain because they are prone to oxidize over time. Corrosion of $Ti_3C_2T_x$ in a hydrogel should be even faster when applied in a working circuit since the applied voltage will speed up corrosion. This issue is critical for the future success of $Ti_3C_2T_x$-based strain sensors. MAVIN provides a solution to this challenge as well because here the $Ti_3C_2T_x$ flakes are protected from oxidation since, due to the absence of solvent, they merely perform as "conductive wire" rather than electron donor under the working conditions.

To investigate the electrochemical stability performance of MAVIN, we prepared also a MXene hydrogel sensor (MHS) with the same $Ti_3C_2T_x$ as described in the Methods section [21], and connected both MAVIN and MHS separately to a 3 V battery, which mimics a commercial button cell (Fig. 5a). After running at ambient temperature for 18 h, the MHS sample revealed two large voids around electrodes and its color turned light, which indicates that the $Ti_3C_2T_x$ flakes were oxidized (Fig. 5b). In contrast, the same conditions didn't cause observable damage or color change on the MAVIN sample (Fig. 5c) and did not change the sensing behavior (Fig. S8).

XPS was carried out to quantify the oxidation process. As demonstrated in Fig. 5d, in the Ti 2$p$ core level spectrum a clear oxide-related peak emerges at a binding energy (BE) of 459.5 eV for MHS after applying 3 V for 18 h. In contrast, there is only an inconspicuous signal at 459.5 eV in our MAVIN sample after the same treatment, which could be caused by the XPS sample preparation (Methods). The XPS data of MAVIN before applying voltage indeed shows that there is already a


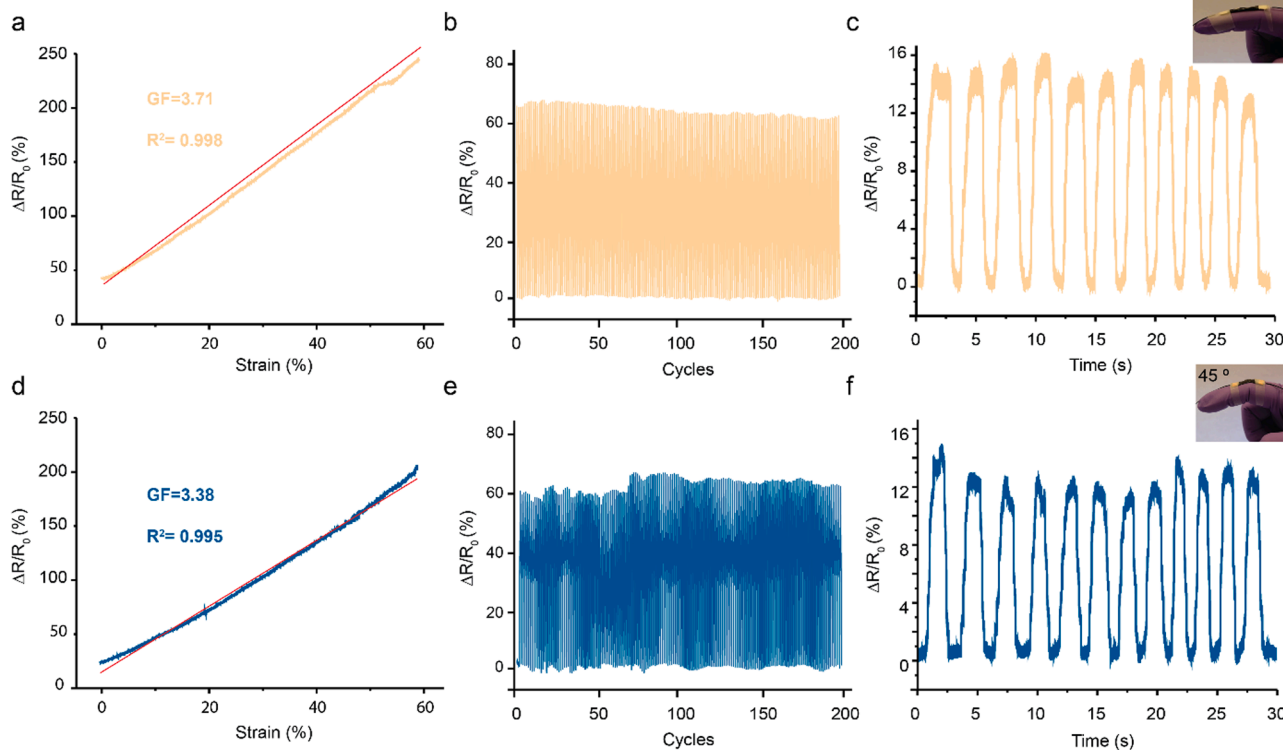
**Fig. 4.** Sensing capability of MAVIN. (Yellow curves: original MAVIN; Blue curves: healed MAVIN) a and d Typical relative resistance−strain curve of a MAVIN strain sensor at a stretching rate of 30 mm min$^{-1}$. b and e Durability test under a strain of 20 % at a stretching rate of 30 mm min$^{-1}$. c and f Resistance change of original and healed MAVIN in response to finger bending (45°).
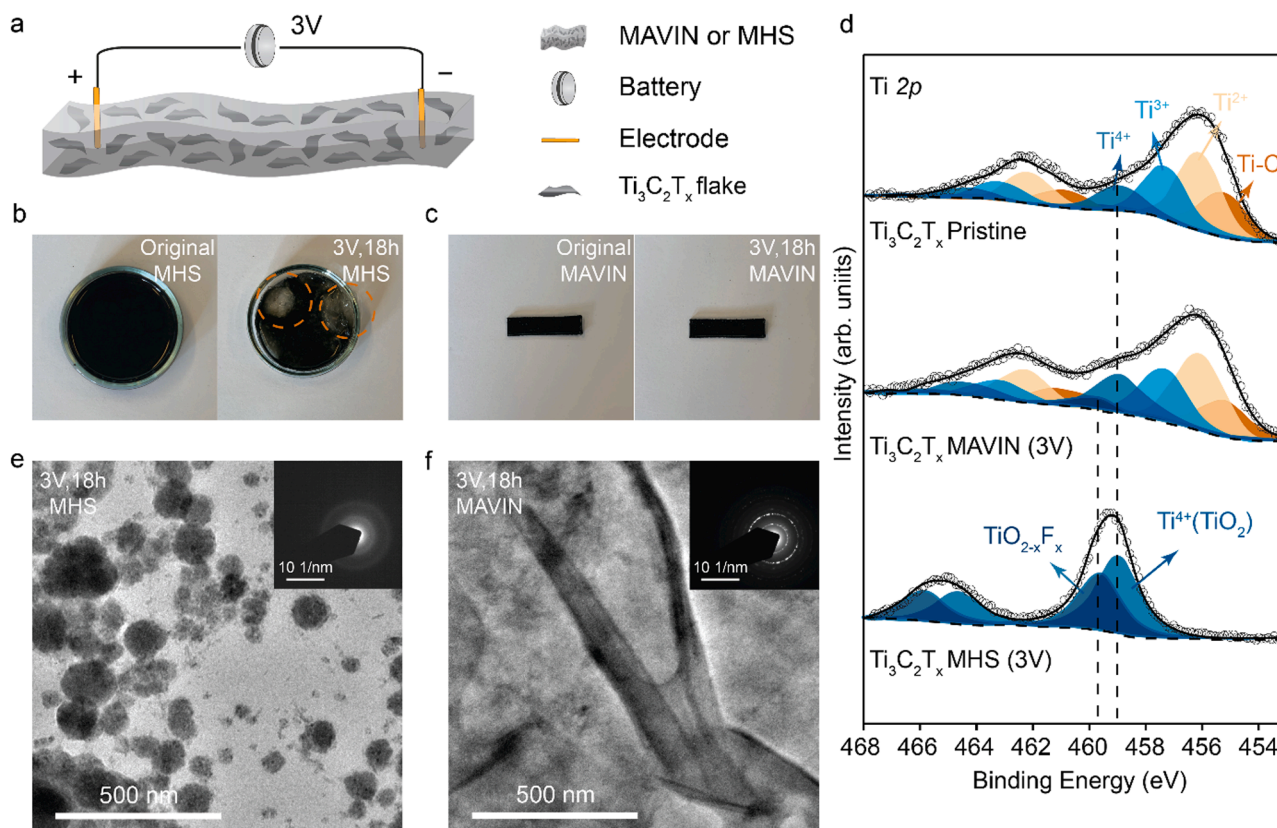
**Fig. 5.** Oxidation tolerant performance of MAVIN compared to MHS. a Schematic illustration of the working circuit for oxidation tests of MXene hybrid materials (MHS or MAVIN); b and c photographs of MHS and MAVIN before and after applying 3 V for 18 h; d XPS spectra of the Ti2$p$ core level region of pristine MXene, MXene in MAVIN and in MHS after applying 3 V for 18 h. e and f high-resolution TEM images of MHS and MAVIN after applying 3 V for 18 h (Inset: Corresponding SAED of beads (e) and flakes (f)).

slight oxidation of $Ti_3C_2T_x$, which must have taken place during depolymerization of MAVIN at 55 °C (Fig. S9) [43,60].

The TEM results (Fig. 5e) show that for the MHS sample the flake structure of $Ti_3C_2T_x$ disappeared and bead-like oxides formed. The crystalline structure typical for $Ti_3C_2T_x$ is recognized for in the SAED pattern of MAVIN (Fig. 5e), while the SAED of MHS testifies to an anamorphous oxide structure. We speculate that the latter is due to the fact that the F-doping breaks up the lattice structure of $TiO_2$ to form amorphous $TiO_{2-x}F_{2x}$ (Fig. 5f) [48].

## 4. Conclusion

High performance strain sensors based on a MXene vitrimer composite material named MAVIN have been successfully developed and applied. Owing to the highly flexible molecular structure of the designed polymer network with abundant hydroxyl groups and dynamic hydrogen bonding between $Ti_3C_2T_x$ flakes and vitrimer matrix, MAVIN accommodated the stretching deformations without deterioration and showed high electromechanical performance. As demonstrated by the impressive electromechanical performance of healed MAVIN, the well-dispersed $Ti_3C_2T_x$ flakes which are strong microwave absorbers, allowed for highly effective healing with a healing speed that is superior to that of any previously reported vitrimer system. Furthermore, the absence of solvent in MAVIN prevents severe oxidation of $Ti_3C_2T_x$ in working conditions, thereby overcoming a major obstacle for self-healing MXene-based strain sensors in practical applications. The strategy presented in this work has demonstrated its effectiveness in design and construction of super stretchable MXene composites with excellent healing capability and oxidation tolerance. Since it effectively eliminates pre-existing limitations of healing MXene hybrid materials,

MAVIN has tremendous potential, not only as a strain sensor but also for artificial skin, soft robots, and human-machine interfacing.

## CRediT authorship contribution statement

**Chongnan Ye:** Methodology, Validation, Formal analysis, Investigation, Data curation, Writing – original draft. **Feng Yan:** Methodology, Validation, Formal analysis, Investigation, Data curation, Writing – original draft. **Xiaohong Lan:** Validation, Formal analysis, Investigation, Writing – review & editing. **Petra Rudolf:** Supervision, Writing – review & editing. **Vincent S.D. Voet:** Conceptualization, Funding acquisition, Supervision, Writing – review & editing. **Rudy Folkersma:** Conceptualization, Funding acquisition, Supervision, Writing – review & editing. **Katja Loos:** Conceptualization, Funding acquisition, Resources, Supervision, Writing – review & editing.

## Declaration of Competing Interest

The authors declare that they have no known competing financial interests or personal relationships that could have appeared to influence the work reported in this paper.

## Data availability

The data that has been used is confidential.

access to the FLIR i7 instrument, Jur van Dijken for help with the thermal and mechanical analysis, Xiaotian Zhu for assistance with TEM and SAED imaging and Dr. Théophile Pelras for critical reading of the manuscript. F. Yan thanks the China Scholarship Council (CSC No. 201704910930) and the University of Groningen for support for his PhD studies. This work benefitted from financial support by the Advanced Materials research program of the Zernike National Research Centre under the Bonus Incentive Scheme of the Dutch Ministry for Education, Culture and Science and by the GreenPAC Polymer Application Centre.

## Supplementary materials

Supplementary material associated with this article can be found, in the online version, at doi:10.1016/j.apmt.2022.101683.

## References

[1] M. Naguib, M. Kurtoglu, V. Presser, J. Lu, J. Niu, M. Heon, L. Hultman, Y. Gogotsi, M.W. Barsoum, Two-dimensional nanocrystals produced by exfoliation of $Ti_3AlC_2$, Adv. Mater. 23 (2011) 4248–4253.

[2] M. Naguib, V.N. Mochalin, M.W. Barsoum, Y. Gogotsi, 25th anniversary article: MXenes: a new family of two-dimensional materials, Adv. Mater. 26 (2014) 992–1005.

[3] Y.H. Li, F. Zhang, Y. Chen, J.Y. Li, Y.J. Xu, Photoredox-catalyzed biomass intermediate conversion integrated with $H_2$ production over Ti3C2Tx/CdS composites, Green Chem. 22 (2020) 163–169.

[4] X. Xie, C. Chen, N. Zhang, Z.R. Tang, J. Jiang, Y.J. Xu, Microstructure and surface control of MXene films for water purification, Nat. Sustain. 2 (2019) 856–862.

[5] P. Xue, H.K. Bisoyi, Y. Chen, H. Zeng, J. Yang, X. Yang, P. Lv, X. Zhang, A. Priimagi, L. Wang, X. Xu, Q. Li, Near-infrared light-driven shape-morphing of programmable anisotropic hydrogels enabled by MXene nanosheets, Angew. Chem. Int. Ed. 60 (2021) 3390–3396.

[6] J. Yang, X. Zhang, X. Zhang, L. Wang, W. Feng, Q. Li, Beyond the visible: bioinspired infrared adaptive materials, Adv. Mater. 33 (2021) e2004754.

[7] M. Yang, Y. Xu, X. Zhang, H.K. Bisoyi, P. Xue, Y. Yang, X. Yang, C. Valenzuela, Y. Chen, L. Wang, W. Feng, Q. Li, Bioinspired phototropic MXene-reinforced soft tubular actuators for omnidirectional light-tracking and adaptive photovoltaics, Adv. Funct. Mater. 32 (26) (2022) 2201884.

[8] X. Zhang, Y. Yang, P. Xue, C. Valenzuela, Y. Chen, X. Yang, L. Wang, W. Feng, Three-dimensional electrochromic soft photonic crystals based on MXene-integrated blue phase liquid crystals for bioinspired visible and infrared camouflage, Angew. Chem. Int. Ed. 61 (42) (2022), e202211030.

[9] X. Liang, A. Garsuch, L.F. Nazar, Sulfur cathodes based on conductive MXene nanosheets for high-performance lithium-sulfur batteries, Angew. Chem. Int. Ed. 54 (2015) 3907–3911.

[10] B. Ahmed, D.H. Anjum, Y. Gogotsi, H.N. Alshareef, Atomic layer deposition of SnO 2 on MXene for Li-ion battery anodes, Nano Energy 34 (2017) 249–256.

[11] G.S. Gund, J.H. Park, R. Harpalsinh, M. Kota, J.H. Shin, T.I. Kim, Y. Gogotsi, H. S. Park, MXene/polymer hybrid materials for flexible AC-filtering electrochemical capacitors, Joule 3 (2019) 164–176.

[12] X. Wang, S. Kajiyama, H. Iinuma, E. Hosono, S. Oro, I. Moriguchi, M. Okubo, A. Yamada, Pseudocapacitance of MXene nanosheets for high-power sodium-ion hybrid capacitors, Nat. Commun. 6 (2015) 6544.

[13] R. Li, X. Ma, J. Li, J. Cao, H. Gao, T. Li, X. Zhang, L. Wang, Q. Zhang, G. Wang, C. Hou, Y. Li, T. Palacios, Y. Lin, H. Wang, X. Ling, Flexible and high-performance electrochromic devices enabled by self-assembled 2D TiO2/MXene heterostructures, Nat. Commun. 12 (2021) 1587.

[14] G. Gao, A.P. O'Mullane, A. Du, 2D MXenes: a new family of promising catalysts for the hydrogen evolution reaction, ACS Catal. 7 (2016) 494–500.

[15] J. Ran, G. Gao, F.T. Li, T.Y. Ma, A. Du, S.Z. Qiao, Ti3C2 MXene co-catalyst on metal sulfide photo-absorbers for enhanced visible-light photocatalytic hydrogen production, Nat. Commun. 8 (2017) 13907.

[16] Y. Cai, J. Shen, G. Ge, Y. Zhang, W. Jin, W. Huang, J. Shao, J. Yang, X. Dong, Stretchable $Ti_3C_2T_x$ MXene/carbon nanotube composite based strain sensor with ultrahigh sensitivity and tunable sensing range, ACS Nano 12 (2018) 56–62.

[17] D. Chen, Q. Pei, Electronic muscles and skins: a review of soft sensors and actuators, Chem. Rev. 117 (2017) 11239–11268.

[18] P. Lv, X. Yang, H.K. Bisoyi, H. Zeng, X. Zhang, Y. Chen, P. Xue, S. Shi, A. Priimagi, L. Wang, W. Feng, Q. Li, Stimulus-driven liquid metal and liquid crystal network actuators for programmable soft robotics, Mater. Horiz. 8 (2021) 2475–2484.

[19] G.Z. Yang, J. Bellingham, P.E. Dupont, P. Fischer, L. Floridi, R. Full, N. Jacobstein, V. Kumar, M. McNutt, R. Merrifield, B.J. Nelson, B. Scassellati, M. Taddeo, R. Taylor, M. Veloso, Z.L. Wang, R. Wood, The grand challenges of science robotics, Sci. Robot. 3 (2018) eaar7650.

[20] Y.Z. Zhang, K.H. Lee, D.H. Sougrat, R. Sougrat, Q. Jiang, H. Kim, H.N. Alshareef, MXenes stretch hydrogel sensor performance to new limits, Sci. Adv. 4 (6) (2018) eaat0098.

[21] H. Liao, X. Guo, P. Wan, G. Yu, Conductive MXene nanocomposite organohydrogel for flexible, healable, low-temperature tolerant strain sensors, Adv. Funct. Mater. 29 (39) (2019) 1904507.

[22] C. Ma, M.G. Ma, C. Si, X.X. Ji, P. Wan, Flexible MXene-based composites for wearable devices, Adv. Funct. Mater. 31 (22) (2021) 2009524.

[23] K. Zhang, J. Sun, J. Song, C. Gao, Z. Wang, C. Song, Y. Wu, Y. Liu, Self-Healing Ti3C2 MXene/PDMS supramolecular elastomers based on small biomolecules modification for wearable sensors, ACS Appl. Mater. Interfaces 12 (2020) 45306–45314.

[24] J. Zhang, L. Wan, Y. Gao, X. Fang, T. Lu, L. Pan, F. Xuan, Highly stretchable and self-healable MXene/polyvinyl alcohol hydrogel electrode for wearable capacitive electronic skin, Adv. Electron. Mater. 5 (7) (2019) 1900285.

[25] T.S.M. JunTang, N. Kurra, A. Sarycheva, X.U Xiao, M.N. Hedhili, Q. Jiang, H. N. Alshareef, B. Xu, F. Pan, Y. Gogotsi, Tuning the electrochemical performance of titanium carbide MXene by controllable *in situ* anodic oxidation, Angew. Chem. Int. Ed. 58 (2019) 7.

[26] H. Lei, L. Dong, Y. Li, J. Zhang, H. Chen, J. Wu, Y. Zhang, Q. Fan, B. Xue, M. Qin, B. Chen, Y. Cao, W. Wang, Stretchable hydrogels with low hysteresis and anti-fatigue fracture based on polyprotein cross-linkers, Nat. Commun. 11 (2020) 4032.

[27] Z. Wang, Y. Liu, D. Zhang, K. Zhang, C. Gao, Y. Wu, Tough, stretchable and self-healing C-MXenes/PDMS conductive composites as sensitive strain sensors, Compos. Sci. Technol. 216 (10) (2021) 109042.

[28] J. Ma, Y. Yang, C. Valenzuela, X. Zhang, L. Wang, W. Feng, Mechanochromic, shape-programmable and self-healable cholesteric liquid crystal elastomers enabled by dynamic covalent boronic ester bonds, Angew. Chem. Int. Ed. 61 (2022), e202116219.

[29] M.C. Damien Montarnal, F. Tournilhac, L. Leibler, Silica-like malleable materials from permanent organic networks, Science 334 (6058) (2011) 965–968.

[30] P.R. Christensen, A.M. Scheuermann, K.E. Loeffler, B.A. Helms, Closed-loop recycling of plastics enabled by dynamic covalent diketoenamine bonds, Nat. Chem. 11 (2019) 442–448.

[31] Z. Pei, Y. Yang, Q. Chen, E.M. Terentjev, Y. Wei, Y. Ji, Mouldable liquid-crystalline elastomer actuators with exchangeable covalent bonds, Nat. Mater. 13 (2014) 36–41.

[32] A. Ruiz de Luzuriaga, R. Martin, N. Markaide, A. Rekondo, G. Cabañero, J. Rodríguez, I. Odriozola, Epoxy resin with exchangeable disulfide crosslinks to obtain reprocessable, repairable and recyclable fiber-reinforced thermoset composites, Mater. Horiz. 3 (2016) 241–247.

[33] P. Shieh, W. Zhang, K.E.L. Husted, S.L. Kristufek, B. Xiong, D.J. Lundberg, J. Lem, D. Veysset, Y. Sun, K.A. Nelson, D.L. Plata, J.A. Johnson, Cleavable comonomers enable degradable, recyclable thermoset plastics, Nature 583 (2020) 542–547.

[34] C. Ye, V.S.D. Voet, R. Folkersma, K. Loos, Robust superamphiphilic membrane with a closed-loop life cycle, Adv. Mater. 33 (2021) e2008460.

[35] Z. Pei, Y. Yang, Q. Chen, Y. Wei, Y. Ji, Regional shape control of strategically assembled multishape memory vitrimers, Adv. Mater. 28 (2016) 156–160.

[36] G. Zhao, Y. Zhou, J. Wang, Z. Wu, H. Wang, H. Chen, Self-healing of polarizing films via the synergy between gold nanorods and vitrimer, Adv. Mater. 31 (2019), e1900363.

[37] F. Lossada, D. Jiao, D. Hoenders, A. Walther, Recyclable and light-adaptive vitrimer-based nacre-mimetic nanocomposites, ACS Nano 15 (2021) 5043–5055.

[38] F. Lossada, B. Zhu, A. Walther, Dry processing and recycling of thick nacre–mimetic nanocomposites, Adv. Funct. Mater. 31 (30) (2021) 2102677.

[39] N. Zheng, Y. Xu, Q. Zhao, T. Xie, Dynamic covalent polymer networks: a molecular platform for designing functions beyond chemical recycling and self-healing, Chem. Rev. 121 (2021) 1716–1745.

[40] M. Capelot, D. Montarnal, F. Tournilhac, L. Leibler, Metal-catalyzed transesterification for healing and assembling of thermosets, J. Am. Chem. Soc. 134 (2012) 7664–7667.

[41] M.L. Goldberger, K.M. Watson, Collision Theory, Courier Corporation, 2004.

[42] M. Guerre, C. Taplan, J.M. Winne, F.E. Du Prez, Vitrimers: directing chemical reactivity to control material properties, Chem. Sci. 11 (2020) 4855–4870.

[43] C.J. Zhang, S. Pinilla, N. McEvoy, C.P. Cullen, B. Anasori, E. Long, S.H. Park, A. Seral-Ascaso, A. Shmeliov, D. Krishnan, C. Morant, X. Liu, G.S. Duesberg, Y. Gogotsi, V. Nicolosi, Oxidation stability of colloidal two-dimensional titanium carbides (MXenes), Chem. Mater. 29 (2017) 4848–4856.

[44] Y. Qing, W. Zhou, F. Luo, D. Zhu, Titanium carbide (MXene) nanosheets as promising microwave absorbers, Ceram. Int. 42 (2016) 16412–16416.

[45] O. Ivashenko, H. Logtenberg, J. Areephong, A.C. Coleman, P.V. Wesenhagen, E. M. Geertsema, N. Heureux, B.L. Feringa, P. Rudolf, W.R. Browne, Remarkable stability of high energy conformers in self-assembled monolayers of a bistable electro- and photoswitchable overcrowded alkene, J. Phys. Chem. C 115 (2011) 22965–22975.

[46] J.F. Moulder, W.F. Stickle, P.E. Sobol, K.D. Bomben. Handbook of X-ray Photoelectron Spectroscopy, Pelmir-Elmer Corporation, Minnesota, 1992.

[47] W. Bao, L. Liu, C. Wang, S. Choi, D. Wang, G. Wang, Facile synthesis of crumpled nitrogen-doped MXene nanosheets as a new sulfur host for lithium-sulfur batteries, Adv. Energy Mater. 8 (13) (2018) 1702485.

[48] V. Natu, M. Benchakar, C. Canaff, A. Habrioux, S. Célérier, M.W. Barsoum, A critical analysis of the X-ray photoelectron spectra of Ti3C2Tz MXenes, Matter 4 (2021) 1224–1251.

[49] H. Li, Y. Hou, F. Wang, M.R. Lohe, X. Zhuang, L. Niu, X. Feng, Flexible all-solid-state supercapacitors with high volumetric capacitances boosted by solution processable MXene and electrochemically exfoliated graphene, Adv. Energy Mater. 7 (4) (2017) 1601847.

[50] K. Parida, G. Thangavel, G. Cai, X. Zhou, S. Park, J. Xiong, P.S. Lee, Extremely stretchable and self-healing conductor based on thermoplastic elastomer for all-three-dimensional printed triboelectric nanogenerator, Nat. Commun. 10 (2019) 2158.

[51] J.C. Lai, X.Y. Jia, D.P. Wang, Y.B. Deng, P. Zheng, C.H. Li, J.L. Zuo, Z. Bao, Thermodynamically stable whilst kinetically labile coordination bonds lead to strong and tough self-healing polymers, Nat. Commun. 10 (2019) 1164.

[52] P. Wei, T. Chen, G. Chen, H. Liu, I.T. Mugaanire, K. Hou, M. Zhu, Conductive self-healing nanocomposite hydrogel skin sensors with antifreezing and thermoresponsive properties, ACS Appl. Mater. Interfaces 12 (2020) 3068–3079.

[53] D.J. Fortman, J.P. Brutman, C.J. Cramer, M.A. Hillmyer, W.R. Dichtel, Mechanically activated, catalyst-free polyhydroxyurethane vitrimers, J. Am. Chem. Soc. 137 (2015) 14019–14022.

[54] C. He, S. Shi, D. Wang, B.A. Helms, T.P. Russell, Poly(oxime-ester) vitrimers with catalyst-free bond exchange, J. Am. Chem. Soc. 141 (2019) 13753–13757.

[55] W.X. Liu, C. Zhang, H. Zhang, N. Zhao, Z.X. Yu, J. Xu, Oxime-based and catalyst-free dynamic covalent polyurethanes, J. Am. Chem. Soc. 139 (2017) 8678–8684.

[56] M.M. Obadia, B.P. Mudraboyina, A. Serghei, D. Montarnal, E. Drockenmuller, Reprocessing and recycling of highly cross-linked ion-conducting networks through transalkylation exchanges of C-N bonds, J. Am. Chem. Soc. 137 (2015) 6078–6083.

[57] H. Ying, Y. Zhang, J. Cheng, Dynamic urea bond for the design of reversible and self-healing polymers, Nat. Commun. 5 (2014) 3218.

[58] Z. Ma, S. Li, H. Wang, W. Cheng, Y. Li, L. Pan, Y. Shi, Advanced electronic skin devices for healthcare applications, J. Mater. Chem. B 7 (2019) 173–197.

[59] M. Xin, J. Li, Z. Ma, L. Pan, Y. Shi, MXenes and their applications in wearable sensors, Front. Chem. 8 (2020) 297.

[60] H. Ghassemi, W. Harlow, O. Mashtalir, M. Beidaghi, M.R. Lukatskaya, Y. Gogotsi, M.L. Taheri, *In situ* environmental transmission electron microscopy study of oxidation of two-dimensional Ti$_3$C$_2$ and formation of carbon-supported TiO$_2$, J. Mater. Chem. A 2 (2014) 14339–14343.